buildings

MDPI

Article

Adjustable PV Slats for Energy Efficiency and Comfort Improvement of a Radiantly Cooled Office Room in Tropical Climate

Pipat Chaiwiwatworakul

The Joint Graduate School of Energy and Environment, King Mongkut's University of Technology Thonburi, Bangkok 10140, Thailand; pipat.cha@kmutt.ac.th

Abstract: This paper investigated an application of adjustable photovoltaic (PV) slats to improve the thermal performance of an exposed glazing window and sequentially enhance the energy efficiency and thermal comfort of an office room. Solar radiation and longwave heat gains from a window fitted with PV slats were measured through experiments conducted in an outdoor chamber cooled by a radiant ceiling system. The daylight level at the workplane was also measured inside the chamber. A transient thermal model was developed and validated against experimental data. Using the experimental chamber as a demonstration case, the model revealed that adjusting the slats monthly to fully block direct sunlight could reduce the electrical energy use by 67% compared to a typical office with heat reflective glass windows. However, the electricity generated by the PV slats contributed a minor portion of the overall energy savings. To assess the thermal comfort impact of the PV slats in the room with the radiant cooling, this study utilized radiation asymmetry criteria from ASHRAE Standard 55. Simulations showed that the PV slat-shaded glazing window resulted in a lower asymmetric plane radiant temperature than the unshaded window of heat reflective glass. The adjustable slat system reduced the risk of local discomfort for occupants working near the window in the radiantly cooled office room.

Keywords: shading slats; window heat gain; daylight transmission; lateral radiant asymmetry; tropical climate

check for updates

Citation: Chaiwiwatworakul, P. Adjustable PV Slats for Energy Efficiency and Comfort Improvement of a Radiantly Cooled Office Room in Tropical Climate. *Buildings* **2024**, *14*, 3282. https://doi.org/10.3390/buildings14103282

Academic Editor: Adrian Pitts

Received: 6 September 2024
Revised: 14 October 2024
Accepted: 15 October 2024
Published: 17 October 2024

Copyright: © 2024 by the author. Licensee MDPI, Basel, Switzerland. This article is an open access article distributed under the terms and conditions of the Creative Commons Attribution (CC BY) license (https://creativecommons.org/licenses/by/4.0/).

1. Introduction

The building sector accounted for 37% of global carbon dioxide emissions in 2021 [1]. Energy efficiency enhancement and renewable energy utilization are the key measures to drive the sector towards net zero energy and meet a committed carbon neutrality goal within a targeted timeline [2]. Further advancements in building decarbonization and climate sustainability are being driven by the integration of renewable energy systems, energy storage solutions, and AI-powered innovations [3].

Building envelopes has a significant influence on building energy use. Several technologies have been developed and integrated into building envelopes to enhance the thermal performance. Insulation thickness and external fixed overhang size were optimized for exposed walls of various building types under a Mediterranean climate [4]. In the optimization, the strategic control of the building's air-conditioning was taken into account to maximize the energy savings for today's climate and to sustain efficiency under future, more severe global warming conditions. In addition to the overhangs, green wall systems were explored as an alternative for hot climates, showing considerable energy conservation benefits for cooling and daylighting in buildings. By reducing the surface temperature compared to exposed conventional walls, green walls offer the added advantage of improving local climatic conditions [5]. While the selected literature [2–5] focused on technologies for decarbonizing the building sector, a simulation study [6] reinforced the critical impact of global temperature increases on building energy consumption and indoor conditions. It

projected a significant rise in energy demand, particularly in tropical developing countries, if global temperatures reach 2.0 °C by 2050, above the pre-industrial levels.

In the tropics, solar radiation is intense, natural daylight is abundant, and ambient temperature is aways high all year round [7,8]. Building facades play an important role in conserving building energy by minimizing the heat gain of solar radiation and optimizing the use of natural daylight for indoor lighting [9].

A modern façade of large glass windows and curtain walls has been widely adopted for commercial buildings and now for new residential houses in many tropical countries. However, this facade design is poorly suited to hot and humid climate, as it allows excessive heat to be absorbed and transferred to cooling systems. The current favored solution is to use dark-colored, heat reflective glass. Unfortunately, this approach is not environmentally sustainable as it neglects the potential for natural daylight, leading to a full reliance on electric lighting. In addition, the glass facades have a high solar absorptance, causing a large amount of solar radiation to be absorbed and raise the glass surface temperature. Consequently, such buildings are energy intensive and prone to thermal discomfort [10,11].

Sun shading is an effective technological solution for enhancing the thermal performance of building facades, particularly glass windows. Various installation options have been investigated, including slats installed behind the windows [12,13], in front of the windows [14–16], or configured between two glass panes [17,18]. These slats can either be permanently fixed or adjustable to different angles. Studies, conducted through experiments and simulations, have examined multiple aspects such as thermal and daylight performance, energy-saving potential, and occupant comfort associated with the use of slats.

Daylighting from automatic mini-blinds was experimentally investigated in a chamber under a real tropical climate [19]. In this study, the blinds were installed between two glazed panes of a south-facing window. With the daylight-responsive control, the blind adjustment reduced 70% of the electrical energy compared to solely using electric lamps with uniform lighting. Another recent study in a moderate climate assessed a double-tilted venetian blind system that the blind slats could be set at different angles for the upper and lower section of the window [20]. The experiments demonstrated that this system offered better indoor daylight distribution and visual comfort than the traditional blinds. However, the aforementioned studies examined only the daylighting aspect.

External shading slats are probably superior to the internal blinds, as the solar radiation can be blocked before it reaches the interior and can be absorbed by the glass window. A study with full-scale experiments reported that the daylighting from external horizontal slats equipped with the south window could reduce the energy consumed for lighting and cooling by as much as 60% when it was compared to the same room using an unshaded glass window [21]. A separate study of the same authors also reported that the same application of the external slats for the north window could reduce energy use by 50%, marginally lower than the south-facing window case [22]. The electric saving was evaluated against the reference case to meet the workplane illuminance of 500 lux for the whole indoor space over the office hours 8:00–17:00. The energy assessments in ref. [21,22] covered both the thermal load and daylight transmission from the window equipped with the slats. They remarked that the transmission calculations by the models required the data of both global and diffuse horizontal solar radiation, and the outdoor daylight illuminance.

Building-integrated photovoltaic (BIPV) is a solar power system that functions as part of building envelope and produces electricity from solar radiation. Photovoltaic shading devices (PVSDs) are a class of BIPVs offering combined functions: the solar control, daylighting, and power generation. In a Mediterranean climate, a study examined various fixed external PV shading configurations (e.g., single or double canopies, horizontal or vertical louvers, surrounding shading, etc.), and the analysis recommended the optimal configurations that balanced energy for heating, cooling, and daylighting [23,24]. Another simulation study optimized fixed shading slats to achieve multiple objectives of minimum electricity use, maximal PV generation, and enhanced daylight harvesting by varying

the number of slats together with adjusting the slat angles [25]. However, some studies highlighted that fixed external shading devices offer limited daylight on overcast days and may allow direct solar penetration, leading occupants to likely appreciate adjustable shading slats [26–28].

Daylight from window supplements electric light to illuminate office space. Controlling the daylight is subject to the implemented interior illumination strategy. For an office with uniform lighting, the slats regulate the transmitted daylight amount to meet the workplane illuminance at 500 lux for the whole room. For a case of task-ambient lighting where the two illumination levels are present, the parameters were 300 lux for circulation area and 500 lux for workstations, and the daylight from window is regulated just to meet 300 lux on the workplane level. Table lamps will provide an additional 200 lux to meet the required light level at the workstations

Extensively studied in the tropical region, the radiant cooling is being promoted as a sound air-conditioning technology capable of reducing the largest amount of energy use in commercial office buildings [29–31]. Unlike the conventional mixed air system, the radiant cooling provides human thermal comfort mainly via the radiative heat exchange. Hence, the exposed windows tended to cause the local discomfort to occupants due to the lateral radiant asymmetry, even though the global thermal comfort was already achieved in the radiant cooling spaces [32–34]. Referring to the ASHRAE standard 55 [35], the radiant asymmetry is described as the radiant temperature difference between two opposite sides of a plane. The standard limits the plane radiant temperature difference to 14 °C to ensure the thermal discomfort being less than 5% for the room using the radiantly cooled ceiling. Regarding this, the windows with sun shading potentially improve the thermal comfort and help success the promotion of the radiant cooling.

To support the development of ultra-low energy buildings for decarbonizing the building sector in the tropical region, this paper studied an integrated technology of adjustable photovoltaics (PV) slat system to enhance window thermal performance in radiantly cooled buildings. Physical experiments and model simulations were carried out to assess and compare the lighting and cooling energy use of a room using the window with PV slats against the room with the unshaded glass window. The power generation from the PV slats was also considered. Referring to the prior author's work [19], a thermal model was developed for a Venetian blind system enclosed between two panes of glass. The model used three external variables—global solar radiation, diffuse horizontal radiation, and sky radiance distribution patterns—to calculate the window solar transmission and heat gain accurately. In this study, a simplified thermal model was introduced for an external PV slat system installed with a double-glazed window. This model streamlined the calculations by using only the vertical solar radiation incident on the windowed wall, reducing the amount of input data needed. The simplified approach allowed for easier integration into a computerized control system for the PV slats. Moreover, as the PV slat system was paired with a radiant cooling system, the heat transfer through the window was calculated based on both the mean radiant temperature and the air temperature inside the room. From a thermal comfort perspective, the study also evaluated the occupant acceptance of the PV slat technology in buildings with radiant cooling. Although the radiant cooling system perfectly maintained overall thermal comfort, the local discomfort caused by radiative heat from high-temperature window surfaces was analyzed using the plane radiant temperature difference metric. The findings demonstrated that a simple slat adjustment strategy to block direct sunlight significantly reduced both cooling and lighting energy consumption while minimizing the local thermal discomfort in the radiant-cooled environment.

2. Materials and Methods

A system of adjustable PV slats equipped with a double-pane glass window was studied under real climate conditions to measure the thermal and the daylight transmissions. A mathematical model was also developed for the PV slat system and validated against

experimental data. This model was then used to assess the energy saving potential for a demonstration case of an office room with the PV slat system.

2.1. The PV Slat System

By applying the knowledge base from our past research of the mini blinds enclosed by the two glass panes of a window [19], the heat transfer of the external PV slat system was analyzed and modeled. As shown in Figure 1, the slats had a width W_l, and a gap S_l between two adjacent slats. The PV cells were attached on the lower part of the slat surfaces. The slats were tilted at an angle φ_l to intercept the direct sunlight from the window incidence.

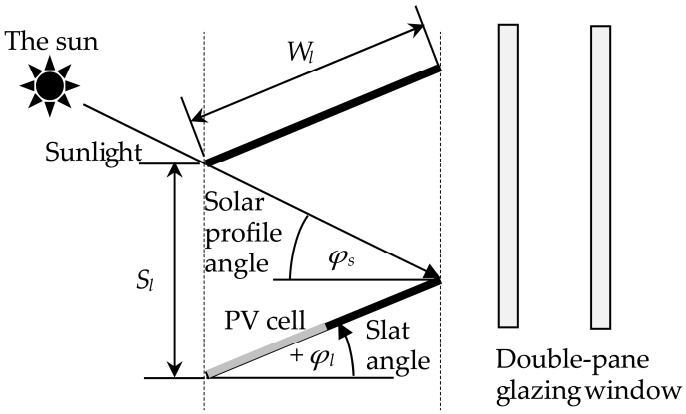


Figure 1. The PV slat system.

For adjusting the slats, solar profile angle (φ_s) is used to specify the direction of sunlight relative to the window plane of the slat system. Here, the profile angle is defined as a geometrical angle between the window normal vector and the projection of the solar vector on the vertical plane that contains the window normal vector. Equation (1) expresses the mathematic function to calculate the profile angle:

$$\varphi_s = \tan^{-1}\left(\frac{\tan \alpha_s}{\cos(\gamma_s - \gamma_W)}\right). \quad (1)$$

In the equation, α_s is solar altitude angle, and γ_s is solar azimuth angle. γ_W is azimuth angle of the window. The PV slats of this system could be adjusted from the fully open position (0 degree to the horizon) to the fully close position (about 70 degrees from the horizon). In practice, the slats had an allowable adjustment range, with a minimum angle called slat critical angle (φ_c), to ensure that the sunlight is fully shaded through the whole considered period of a day, for instance, during office hours. Figure 1 also exhibits the situation of the slats at the critical angle. It is remarked that the slat angle is measured counterclockwise from the horizontal axis to the back surface of the slats.

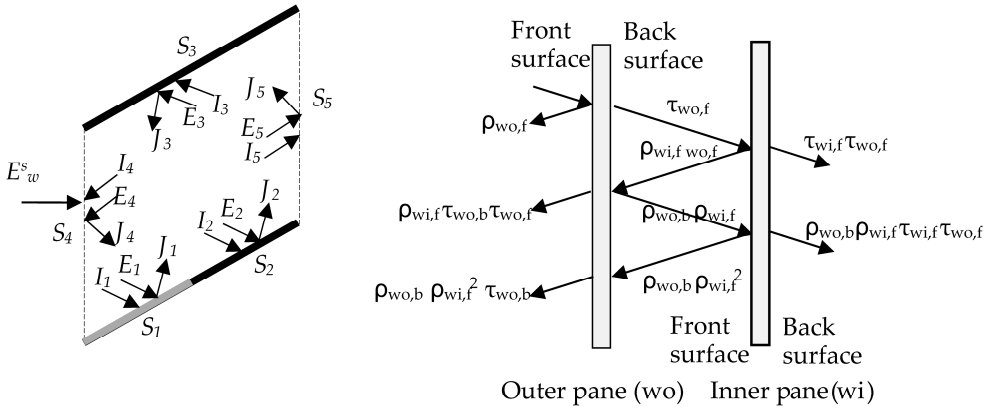
2.2. System Heat Transfer

The heat transfer of the PV slat system was analyzed based on the solar and the thermal radiation exchanges and the heat convection. A system energy balance was performed to determine the net energy absorption of the slats and the window glasses, and the resultant temperature. In the analysis, the surrounding factors influencing the system included the solar radiation, ambient temperature, and room air temperature. Thermal properties of the slat and glass materials also affected the system's heat transfer.

(a) Solar radiation exchange

The solar radiation exchange between the two adjacent PV slats and window was analyzed within a fictive cavity (see Figure 2a). Surfaces S_1, S_2, and S_3 of the cavity represent the PV cell section, the slat upper surface, and the slat lower surface, respectively.

Solar reflectance of the surfaces was correspondent to that of the PV cells and the slat surfaces. S_4 is an imaginary surface with zero reflectance, and S_5 represents the front surface of the outer glass pane of the window.



(**a**) PV slats. (**b**) Glazing window.

Figure 2. Solar radiation exchange of the PV slat system.

The solar radiation normal to the window plane (E^s_w) entered the cavity. Multiple reflections of the radiation undertook inside the cavity until its entire energy was absorbed by the five surfaces (S_1–S_5). The radiosity method as expressed by Equation (2) was applied to determine the reflections and the final solar radiosity of all cavity surfaces (J^s_i):

$$J^s_i = \rho^s_i \cdot I^s_i + \rho^s_i \sum_{j=1}^{n} F_{ij} \cdot J^s_j. \tag{2}$$

In Equation (2), subscript of individual variables i and j is used to identify the cavity surfaces. ρ^s_i is the surface solar reflectance. F_{ij} is the geometrical form factor between two surfaces i and j. I^s_i is the initial incident solar radiation (W_{th}/m^2), determined by multiplying E^s_w with the form factor of surface S_4 to surface i. In this case, initial incident radiation of surface S_4 (I^s_4) was zero.

This calculation also assumed all the surfaces to be diffusive. As a step of this analysis, the received solar radiation on surface i (E^s_i) and the corresponding absorbed energy (A^s_i) could be computed by the two equations below:

$$E^s_i = \sum_i F_{ij} \cdot J^s_i, \text{ and} \tag{3}$$

$$A^s_i = \alpha_i \cdot E^s_i, \tag{4}$$

where α_i is the surface solar absorptance. The calculated values of surface S_5 are the correspondent values of the front surface of the window outer glass pane, e.g., $J^s_{wo,f} = J^s_5$. Subscript *wo,f* stands for the front surface of the outer glass. The calculated values for the slats could be obtained by averaging the values of surfaces S_1 to S_3 weighted by their surface length.

The double-pane glass window formed a part of the slat system. The solar radiation from the fictive cavity ($E^s_{wo,f}$) transmitted through the window outer glass. In Figure 2b, the multiple solar reflections occurred within the air gap enclosed by the two glass panes. Equations (5) and (6) express the amount of the incident radiation on the back surface of the outer glass ($E^s_{wo,b}$) and the front surface of the inner glass panes ($E^s_{wi,f}$), respectively:

$$E^s_{wo,b} = \frac{\rho^s_{wi,f} \cdot \tau^s_{wo,f}}{1 - \rho^s_{wo,b} \cdot \rho^s_{wi,f}} \cdot E^s_{wo,f}, \text{ and} \tag{5}$$

$$E^s_{wi,f} = \frac{\tau^s_{wo,f}}{1 - \rho^s_{wo,b} \cdot \rho^s_{wi,f}} \cdot E^s_{wo,f}. \quad (6)$$

According to the above analysis, the overall solar transmission of the window unit (τ^s_w) can be derived and obtained from Equation (7):

$$\tau^s_w = \frac{\tau^s_{wo,f} \cdot \tau^s_{wi,f}}{1 - \rho^s_{wo,b} \cdot \rho^s_{wi,f}}, \quad (7)$$

where $\tau^s_{wo,f}$ and $\tau^s_{wi,f}$ are the front solar transmittance of the outer and the inner glasses. $\rho^s_{wo,b}$ and $\rho^s_{wi,f}$ are the back solar reflectance of the outer glass and the front solar transmittance of the inner glass. The front solar reflectance of the double-pane window could be determined by using Equation (8) which is also the reflectance of the cavity surface S_5 in Figure 1 and Equation (2):

$$\rho^s_w = \rho^s_{wo,f} + \frac{\tau^s_{wo,f} \cdot \tau^s_{wo,b}}{1 - \rho^s_{wo,b} \cdot \rho^s_{wi,f}}, \quad (8)$$

where $\rho^s_{wo,f}$ and $\rho^s_{wi,f}$ are the front solar reflectance of the outer and inner glass panes, respectively.

(b) Thermal radiative exchange

Analog to the solar radiation exchange, the fictive cavity was applied to analyze the thermal radiative exchange between the slats and the outer glass of the window. By assuming the five surfaces S_1–S_5 to be gray-diffusive, the thermal radiosity (J^t_i) could be expressed by Equation (9):

$$J^t_i = \varepsilon_i \sigma T^4_i + (1 - \varepsilon_i) \sum_{j=1}^{n} F_{ij} \cdot J^t_j, \quad (9)$$

where ε_i is the surface emittance. T_i is the surface temperature (K). It is remarked that as the surface temperature are the unknown variable, an iteration technique is essentially applied for obtaining the solution. The net thermal energy absorbed by individual surface (A^t_i) could be then determined by

$$A^t_i = E^t_i - J^t_i, \quad (10)$$

where $E^t_j = \sum_j F_{ij} \cdot J^t_j$.

At this time, the total radiative energy that the slats absorbed (A^r_l) could be known by summing absorbed solar and thermal radiation components:

$$A^r_l = A^s_l + A^t_l. \quad (11)$$

The radiative energy absorbed by the front surface of the window outer glass pane ($A^r_{wo,f}$) was

$$A^r_{wo,f} = A^s_{wo,f} + A^t_{wo,f}. \quad (12)$$

Considering the window air gap, the back surface of the outer glass radiatively exchanges heat with the front surface of the inner glass. Equation (9) was applied to determine the thermal radiosity of these two surfaces, $J^t_{wo,b}$ and $J^t_{wi,f}$. Then, the total absorbed energy of the outer glass due to the shortwave and longwave radiative exchanges on both font and back surfaces could be obtained from Equation (13):

$$A^r_{wo} = \left(A^s_{wo,f} + A^t_{wo,f}\right) + \left(A^s_{wo,b} + A^t_{wo,b}\right). \quad (13)$$

The absorption of radiative energy of the inner glass was determined from Equation (14):

$$A_{wi}^{r} = \left(A_{wi,f}^{s} + A_{wi,f}^{t}\right) + \left(A_{wi,b}^{t}\right). \quad (14)$$

It is remarked that the solar radiation incident on the back surface of the inner windowpane was not considered in the model.

(c) System energy balance

After obtaining the absorbed energy and the surface temperature due to the radiative exchanges, the energy balance of the entire PV slat system was next performed simultaneously at the slats, the outer glass pane, and the inner glass pane. According to Figure 3, the energy balance equations of the three system components were written as Equations (15)–(17).

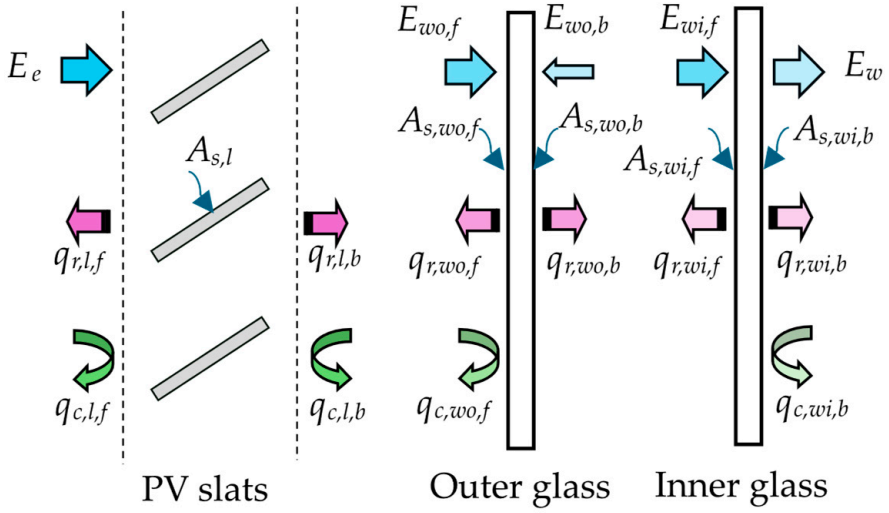


Figure 3. The energy balance of the PV slat system.

– Energy balance at the PV slats

$$A_{l}^{s} + A_{l}^{t} + \frac{T_{l,t} - T_{o}}{R_{\mathrm{c,lo}}} = \frac{\rho_{l} \cdot c_{p,l} \cdot x_{l}}{\Delta t}(T_{l,t} - T_{l,t-1}), \quad (15)$$

– Energy balance at the outer glass

$$A_{wo}^{s} + A_{wo}^{t} + \frac{T_{wo,t} - T_{o}}{R_{c,wo}} = \left(\frac{\rho_{\mathrm{wo}} \cdot c_{p,\mathrm{wo}} \cdot x_{wo}}{\Delta t}\right)(T_{wo,t} - T_{wo,t-1}), \quad (16)$$

– Energy balance at the inner glass

$$A_{wi}^{s} + A_{wi}^{t} + \frac{T_{wi,t} - T_{rm}}{R_{\mathrm{c,wi}}} + \frac{T_{wi,t} - T_{mrt}}{R_{\mathrm{r,wi}}} = \left(\frac{\rho_{\mathrm{wi}} \cdot c_{p,\mathrm{wi}} \cdot x_{\mathrm{wi}}}{\Delta t}\right)(T_{wi,t} - T_{wi,t-1}), \quad (17)$$

According to the equations, surrounding factors influencing the system heat transfer included the outdoor air temperature (T_o), room air temperature (T_{rm}), and room mean radiant temperature (T_{mrt}). As the developed model accounted for the thermal storage effect, the required physical properties of the slat (l) and the outer and the inner glasses (wo and wi) were their density (ρ), specific heat capacity (C_p), and thickness (x). Δt is the calculation time step from time t and $t - 1$. For the model, $R_{c,lo}$ is the thermal resistance of the convective heat transfer between the slats and the outdoor air, assumed at 0.125 $\mathrm{m^2 \cdot K/W}$. $R_{r,lw}$ is the thermal resistance of the radiative heat transfer between the slats and the outer glass.

After determining the temperature values of the three system components, the total heat gain of the PV slat system (q_w) could be calculated as

$$q_w = \tau^s_{wi,f} \cdot E^s_{wi,f} + q_{c,wi,b} + q_{r,wi,b}, \tag{18}$$

where $E^s_{wi,f}$ is the total solar irradiation on the front surface of the inner glass pane. In Equation (18), the convective ($q_{c,wi,b}$) heat and the radiative heat ($q_{r,wi,b}$) between the back surface of the inner glass pane and the room interior can be obtained from

$$q_{c,wi,b} = h_{c,wi} \cdot (T_{wi,t} - T_{rm}), \text{ and} \tag{19}$$

$$q_{r,wi,b} = h_{r,wi} \cdot (T_{wi,t} - T_{rmt}), \tag{20}$$

where $h_{c,wi}$ is the inverse of $R_{c,wi}$, and $h_{r,wi}$ is the inverse of $R_{r,wi}$.

2.3. Daylight Transmission

According to the system configuration, the exterior daylight would travel through the PV slats and the glass window then entering building interior. The overall daylight transmittance (τ^v_{sys}) could be simply determined by multiplying the slat transmittance (τ^v_l) with the window transmittance (τ^v_w):

$$\tau^v_{sys} = \tau^v_l \cdot \tau^v_w. \tag{21}$$

(a) The PV slats

Daylight transmission of the PV slats was complicated due to the slat geometry and the multiple light reflection between two adjacent slats. Analogous to the calculation of Equation (2), flux transfer method was applied to determine the daylight transmission. The diagram in Figure 2 was re-examined in the view of multiple light reflection, instead of solar radiation. The exterior daylight illuminance on the window direction (E^v_w) entered the fictive cavity from surface S_4 and was incident on other surfaces. The luminous exitance (M_i), defined as the daylight flux leaving from the slat and glass surfaces, was calculated by using Equation (22):

$$M_i = M_{di} + \rho^v_i \sum_{j=1}^{n} F_{ij} \cdot M_j, \tag{22}$$

where M_{di} and M_i are the initial and the final exitance of surface, respectively. By solving the multiple linear equations above, the final exitance M_1–M_5 could be obtained. The illuminance or the incident daylight flux on each slat surface (E_i) could be next derived by applying Equation (23):

$$E^v_i = \sum_{j=1}^{n} F_{i \to j} M_j, \tag{23}$$

As surface S_5 represented the outer glass of the window, the daylight transmission of the slat was finally computed from

$$\tau^v_l = \frac{E^v_5}{E^v_w}. \tag{24}$$

(b) The double-pane window

The daylight illuminance from the PV slats next traveled through the double-pane window. The diagram in Figure 2b and Equations (7) and (8) could be applied to determine the light transmittance and reflectance of the window, respectively. However, solar properties of the glass panes were substituted by their visible properties.

2.4. Heat Transfer of a Single Glazing Window

The heat transfer of a single pane glass window was modeled to determine the thermal performance of the heat reflective glass. Figure 4 shows a simple thermal resistance network

of the model. The numerical calculation approach was analogous to the double-pane glass window.

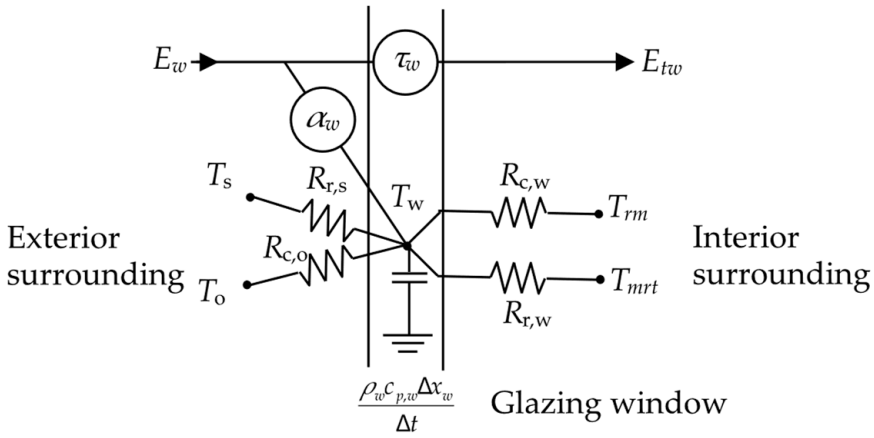


Figure 4. A heat balance model of the single pane glazed window.

2.5. Workplane Daylight Distribution

Daylight from windows can illuminate building rooms. Any points on the workplane level inside the rooms directly received the daylight from windows. Those points also received the reflected daylight from the walls, floors, and ceilings. By applying Equation (25), the workplane daylight illuminance at different points ($E_{wp,i}$) could be determined.

$$E_{wp,i} = E_{wt} \cdot C_i + \sum_{i=1}^{n} M_i \cdot C_i. \quad (25)$$

In Equation (25), the first term represents the direct illuminance from the window, while the second term represents the illuminance reflected from the room's interior surfaces. The variable C_i is a configuration factor of the interior surface and the given point on the workplane. E_{wt} is the transmitted daylight from window. M_i is the final exitance of all interior surfaces derived using the flux transfer method. The detailed calculation was described in our past study [19].

2.6. Experimental Setup

Full scaled experiments were conducted to measure the daylight and solar transmissions and the thermal gain through a window equipped with the PV slats. The proposed model in Section 2 was validated using the measurement results.

(a) Testing chamber

An outdoor chamber was used as the testbed of the PV slat system. The chamber was 3.0 m wide by 9.0 m long with a floor-to-ceiling height of 2.65 m. The chamber had two glass windows: the one on the south-facing wall and the other one on the north-facing wall. Both windows had the same dimension of 2.7 m width by 1.95 m height. The windowsill was 0.70 m above from the floor. All opaque walls of the chamber were insulated by polystyrene foam to reduce the external heat gain. The interior wall surfaces were painted white. Figure 5a exhibits an exterior view of the experimental chamber.

The windows of the chamber were originally a 5.0 mm thick single glass pane. Later, the windows were modified by placing another glass pane behind the existing one, so that the present windows formed a double-pane glazing unit with 7.0 cm thick air gap. The thermal and visible properties of the window glasses were given in Table 1. Properties of a heat reflective glass were also included in the table. It is remarked that the north window was closed and attached with PU foam to form an opaque wall part of the experimental chamber.



(**a**) Exterior view (**b**) Interior view

Figure 5. Experimental chamber.

Table 1. Thermal and visible properties of the glazed windows and the slats.

Description	Typical Window	PV Slat System	
	Heat Reflective	Glass Panes	Slats
Solar transmittance	0.06	0.80	-
Solar reflectance	0.33	0.07	0.68
Solar absorptance	0.61	0.13	0.32
Visible transmittance	0.09	0.89	-
Visible reflectance	0.32	0.08	0.77
Emittance	0.85	0.84	0.85

The chamber simulated an office environment and was conditioned using a radiant ceiling system for cooling (see Figure 5). The radiant ceiling controlled the indoor operative temperature by extracting sensible heat from the chamber envelope (including windows, walls, floor, and roof) and the indoor air. An independent outdoor air unit managed the room's humidity levels by supplying deep dehumidified outside air. The decoupling of the sensible and latent heat extraction offered a precise control of the indoor operative temperature and humidity. Detailed information on the installed radiant system for the experimental chamber can be found in ref. [30].

(b) Adjustable PV slats

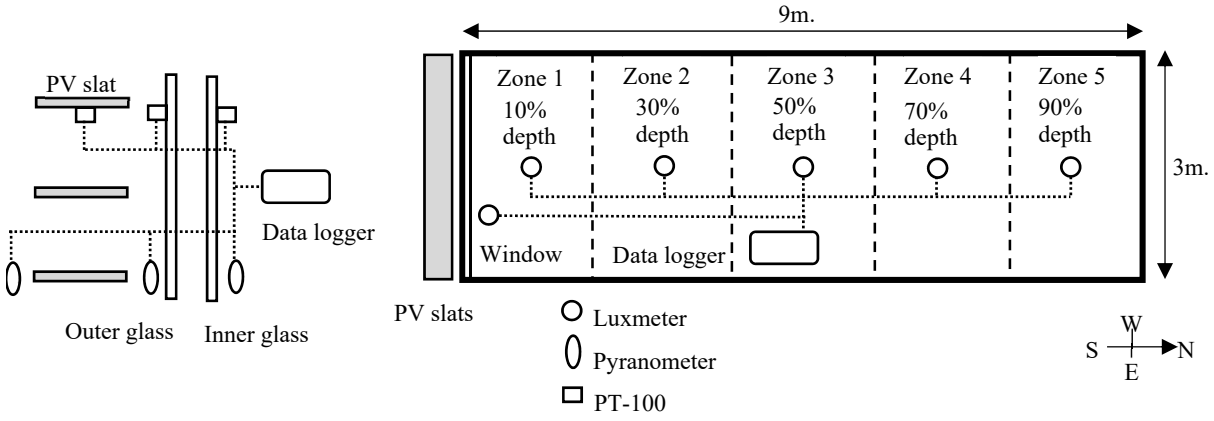
An external adjustable PV slat system was developed and installed on the south-facing window of the chamber (see Figure 5a). The system consisted of seven horizontal slats, each measuring 0.3 m in width and 3.0 m in length, with a 0.25 m gap between adjacent slats. The slats could be adjusted to various angles using an electric linear actuator, controlled online via a computerized controller. The solar and visible properties of the slat surfaces are presented in Table 1.

A total of 154 monocrystalline PV cells were installed on the lower section of the slats' upper surfaces, covering approximately 50% of the slats' surface area. The cells were connected in series to generate power, with each cell rated at 0.37 V and 0.5 A under standard testing conditions. The electricity generated by the PV slats was stored in a battery, which powered the light lamps in the experimental chamber.

(c) Measurements

Measurements were performed to monitor the daylight and thermal conditions in the testing chamber. As shown in Figure 6a, the transmitted solar radiation through the slats and window was measured using two pyranometers (Kipp & Zonen CMP 3): one placed in front of the outer glass pane and the other behind the inner glass pane of the window. The temperature distribution of the slat system was determined using RTD (PT-100) sensors, which measured the surface temperature of a slat and the outer and inner glass panes. A globe thermometer (Lutron WBGT-2010SD) was used to measure the room's air dry-bulb

temperature (T_{rm}), relative humidity (RH_{rm}), and globe temperature (T_g). It is important to note that the outside air temperature was measured at a meteorological station located near the testing chamber.



(**a**) PV slat-window (**b**) testing chamber

Figure 6. Measurement setup.

To assess the daylighting performance, a light sensor (EKO ML020S-O) was used to measure the transmitted daylight amount. Five light sensors were placed to measure the workplane daylight distribution along the room center at 10%, 30%, 50%, 70%, and 90% room depth.

During the experiments, exterior solar radiation and daylight illuminance were measured and recorded at a ground-based solar station (latitude 13.7° N and longitude 100.44° E). The measurements included global, diffuse horizontal, and beam normal components of solar radiation and daylight. Additionally, vertical solar radiation and daylight illuminance were recorded for four orientations: north, east, south, and west. The clock times of the data loggers at both the solar station and the experimental chamber were synchronized, and all data were collected at one-minute intervals.

According to the specifications of the instruments and sensors used in the experiments, the temperature measurement range was between −20 °C and 70 °C, while the relative humidity measurement covered the full range of 0–100%. The readings had a scale resolution of 0.1 °C for temperature and 0.1% for relative humidity. The measurement accuracy was ±0.3 °C for air temperature, ±0.2 °C for globe temperature, and ±3% for relative humidity.

In this experiment campaign, the power generation from the PV cells on the slat surfaces was measured by a built-in logger of a maximum power point tracking (MPPT) solar charging controller for every ten minutes. The incident radiation was simultaneously measured to assess the solar system performance.

3. Results and Discussions

This section presents the experimental results, model validation, and performance assessment of the PV slat application for an office room case.

3.1. Experimental Results

A sequence of the experiments was undertaken by adjusting the slats to specific angles ranging from 0° to 60°, stepping up every 10°. Although the experiments were made on different days, the outdoor conditions remained largely consistent. In this section, only the experiments with the slats set at 0°, 40°, and 60° were selected for discussion. The measurement results were analyzed and used to evaluate accuracy of the model in Section 2.

(a) Slat angle at 0° (fully open)

Figure 7 presents the plots from the experiment of the slats at 0°. The solar radiation on the window orientation ($E_{e,w}$) reached a peak of 600 W_{th}/m^2 at noontime (Figure 7a). The high radiation value resulted from the presence of the beam radiation component, as the sun was traveling due south. However, intermittent cloud cover led to significant fluctuation in the solar radiation throughout the measurement period.

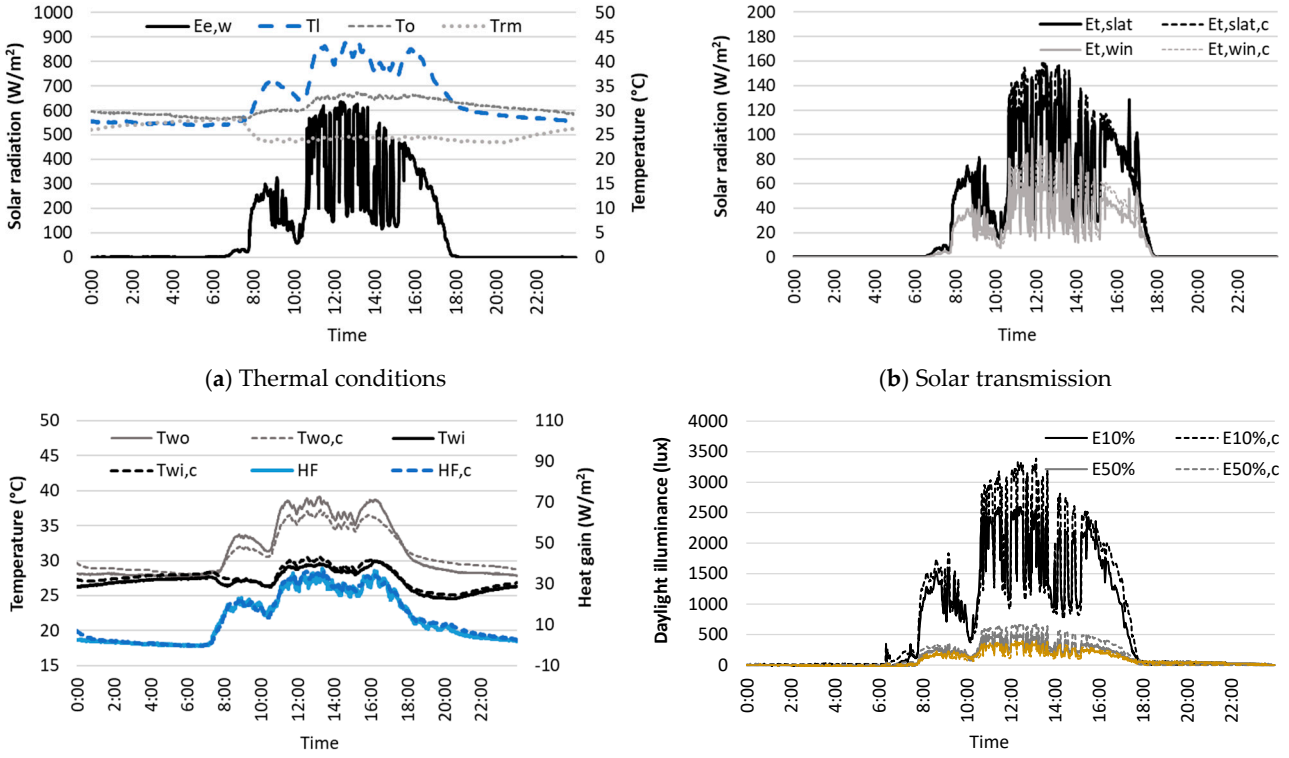


Figure 7. The experimental results of the PV slats at 0°.

The measurements indicated that the diurnal variation of the ambient temperature ranged between 27 and 34 °C. In the daytime, the slat temperature exceeded the ambient temperature due to the absorbed heat from the incident solar radiation. Conversely, during the night, the slats lost heat through radiative exchange with the sky, resulting in lower surface temperatures when it was compared to the ambient temperature.

The air temperature inside the chamber was measured and the results were superimposed on the plot. When the chamber was cooled by the radiant ceiling system (8:00–20:00), the room temperature remained around 24.5 °C. After the radiant system was turned off, the temperature gradually increased. In this study, the four environmental parameters shown in Figure 7a were used as input for the model to assess the performance of the PV slats.

Figure 7b shows the solar radiation measured both in front of the window and behind the window. It is observed that the slats could shade up to 80% of the south-facing solar radiation. The peak solar radiation transmitted into the chamber was only 60 W_{th}/m^2. Additionally, Figure 7b compared the solar radiation calculated using the developed model to the experimental measurements. The subscript c of the variables denoted in the graph plots represents the calculated results obtained from the thermal models. From Table 2, the model accurately predicted the transmitted radiation through the slats ($E_{t,slat}$) with a mean bias difference (MBD) and root mean square difference (RMSD) of 2.24 W_{th}/m^2 and 7.66 W_{th}/m^2, and the transmitted radiation through the window ($E_{t,win}$) with a MBD and RMSD of 1.61 W_{th}/m^2 and 6.94 W_{th}/m^2 for, respectively.

Table 2. Accuracy evaluation of the proposed thermal model.

Parameter	$E_{t,slat}$	$E_{t,win}$	T_{wo}	T_{wi}	HF	$E_{i10\%}$	$E_{i50\%}$	$E_{i90\%}$
				0° slat angle				
MBD	2.24	1.61	−0.16	0.52	0.82	99.1	23.9	−2.5
RMSD	7.66	6.94	1.21	0.57	1.71	281.1	75.3	41.2
				40° slat angle				
MBD	2.31	2.99	−0.31	0.66	1.06	118.9	26.8	−8.7
RMSD	5.45	5.00	1.47	0.69	1.86	194.1	54.9	29.5
				60° slat angle				
MBD	4.12	2.15	−0.40	0.59	0.61	31.1	7.6	−41.7
RMSD	8.14	3.81	1.63	0.65	2.22	105.5	34.3	71.1

Note: $MBD = \frac{1}{N}\sum_{i=1}^{N}(C_i - M_i)$ and $RMSD = \frac{1}{N}\sqrt{\sum_{i=1}^{N}(C_i - M_i)^2}$, where C_i is the calculated value from the model, M_i is the corresponding measured values, and N is the amount of data.

Figure 7c shows the surface temperature of the outer and the inner glass panes of the window, along with the longwave heat gain from the window. The outer glass temperature varied in response to the slat temperature and the solar radiation, peaking at 38 °C around noon and dropping to 28 °C just before sunrise. The inner glass temperature varied between 25 °C and 30 °C. The maximum longwave heat flow (HF) from the window was at 30 W_{th}/m^2. The negative heat gain value during night (0:00–6:00) indicated the heat was flowing outward to the outdoor environment. The calculated glass temperatures and the longwave heat matched the measurements well. It should be remarked that the total heat load from the window was the sum of the transmitted solar radiation through the window and the longwave heat gain.

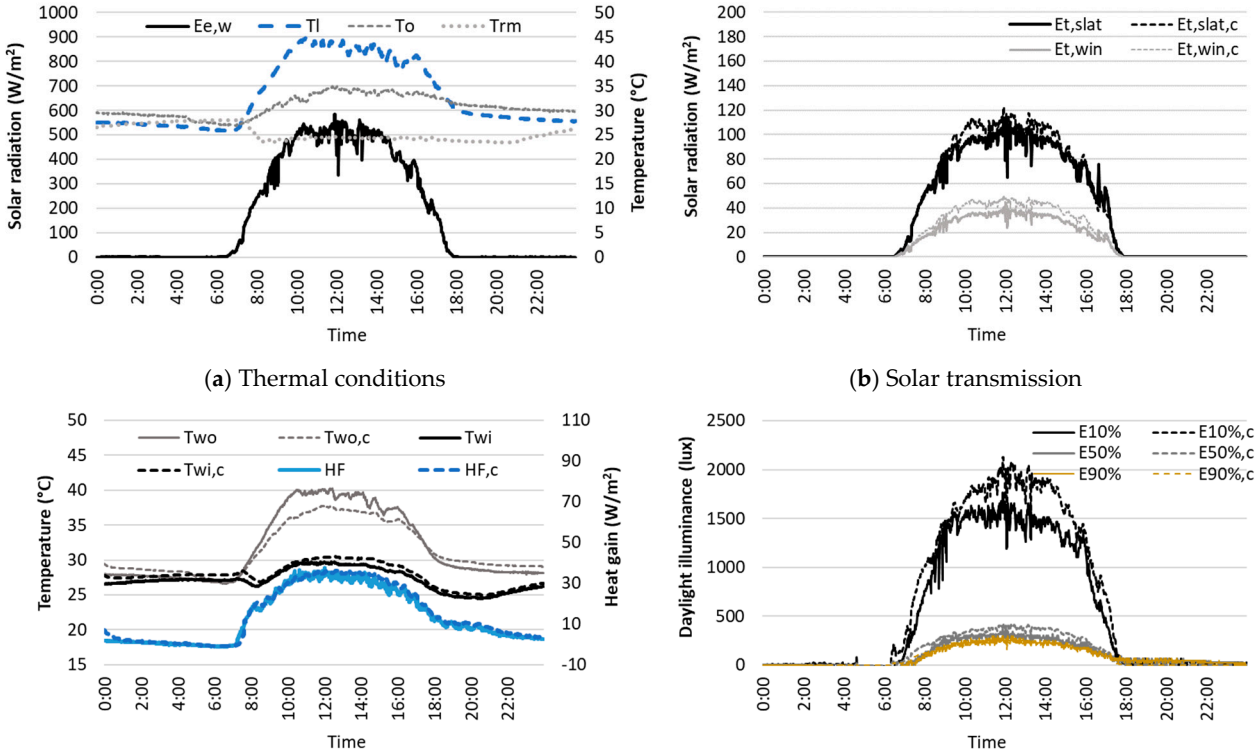
Figure 7d shows the measured daylight illuminance on the workplane at 10%, 50%, and 90% of the room depth (D). The daylight values near the window, (i.e., $E_{i10\%}$) varied between 500 and 2500 lux, which was sufficient for task lighting. Moreover, the daylight could serve the ambient lighting for the whole room for most of the office hours, even though the daylight values sharply decreased, as it extended further into the room depth.

(b) Slat angles at 40°

Figure 8a illustrates the outdoor conditions during the experiment with the slats at a 40° angle. Compared to the previous experiment (0° slat angle), the solar radiation in this case showed less fluctuation, but the peak values remained similar, around 600 W_{th}/m^2. The ambient temperature ranged between 28 and 35 °C, with the room temperature observed to be marginally higher by about 0.3 °C.

Figure 8b presents the transmitted solar radiation through the slats and the window. Due to the increased slat angle providing more shading, solar transmission decreased compared to the previous experiment. Figure 8c shows the temperature distribution of the glass window from the measurements. The plot indicates that temperature variation was primarily influenced by solar radiation transmission. The inner glass pane temperature fluctuated between 26 and 30 °C. Consequently, the longwave heat gain from the window was similar to that of the first experiment (with a 0° slat angle). Therefore, the change in total heat gain from the window was mainly due to the transmitted solar radiation.

Figure 8d presents the workplane daylight illuminance measurements. Near the window, daylight levels exceeded 500 lux, which was sufficient for task lighting throughout the entire working hours. Moving deeper into the middle and rear zones of the chamber, daylight levels decreased to 250–300 lux, which remained adequate for ambient lighting. The plots in Figure 8d demonstrate that the workplane illuminance calculated from the thermal model closely matched the experimental measurements, indicating good model accuracy.



(**a**) Thermal conditions

(**b**) Solar transmission

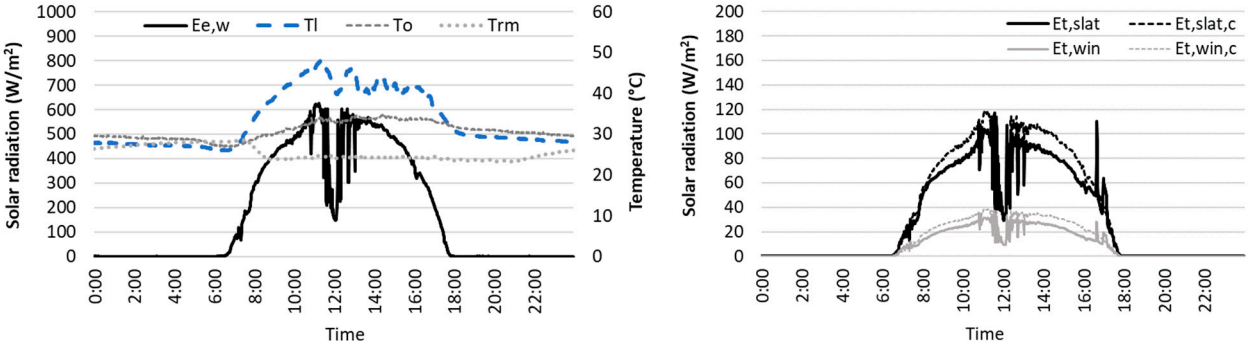
(**c**) Window temperature distribution

(**d**) Workplane daylight illuminance

Figure 8. The experimental results of the PV slats at 40°.

(c) Slat angles at 60° (fully closed)

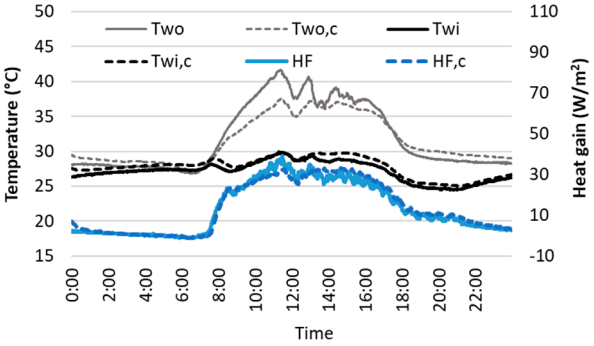
Although the slats were fully closed, there were still small gaps between adjacent slats that allowed the solar radiation and daylight to enter. In Figure 9a, the solar radiation and outdoor temperature in this experiment was not very distinct from the previous two experiments. The solar transmission through the slats and the whole window system was the lowest among all experiments, as shown in Figure 9b. Despite this reduction, the longwave heat gain remained unchanged, which is evident from Figure 9c. In terms of daylighting, Figure 9d indicates that the daylight illuminance slightly decreased compared to the second experiment; however, it remained high near the window.



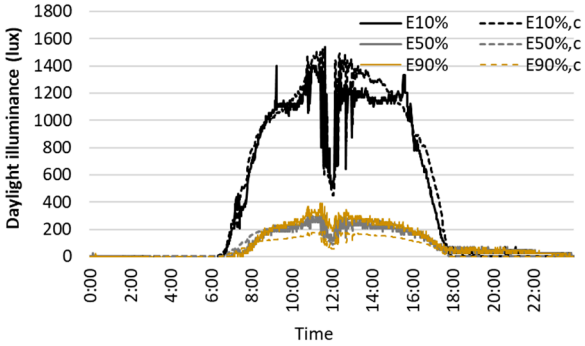
(**a**) Thermal conditions

(**b**) Solar transmission

Figure 9. *Cont.*



(**c**) Window temperature distribution



(**d**) Workplane daylight illuminance

Figure 9. The experimental results of the PV slats at 60°.

(d) Solar power from the PV slats

Figure 10 illustrates the relationship between solar power generation and the incident radiation on the PV slats. During the experiment, the maximum power recorded was 80 W_{elec}. The system was activated and began generating the power only when the incident radiation exceeded 200 W/m^2.

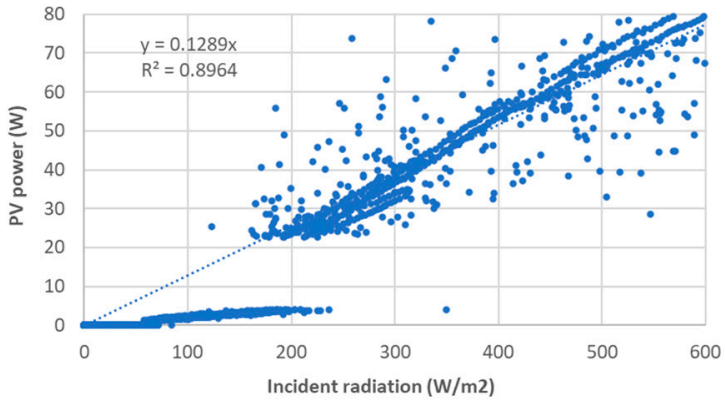


Figure 10. Measurement of the solar power from the PV slats.

Equation (26) expresses the relationship between the PV power (E_{pv}) and incident radiation in relation to the slats (E_l^s):

$$E_{pv} = 0.129 \cdot E_l^s, \text{ if } E_l^s > 200\ W_{th}/m^2. \quad (26)$$

3.2. Performance Assessment

The lighting and cooling energy consumption of an office room equipped with PV slats was assessed and compared to that of a similar room with typical non-shaded windows. The improvement in thermal comfort provided by the slat system was evaluated using the metric of lateral radiant asymmetry. The experimental chamber served as the test environment, with four key parameters considered in the evaluation.

(a) Lighting load

Uniform light distribution by ceiling-mounted lamps was the design norm for office buildings. Light-emitting diode (LED) lamps are fully commercialized with a luminous efficacy (L_f/P) of about 100 lumen/W_{elec}. Using the lumen method, the electrical power density (*LPD* or *P*/*A*) of the interior lighting could be determined from

$$E_{wp} = (LLF)(CU)\left(\frac{L_f}{P}\right)\left(\frac{P}{A_f}\right), \quad (27)$$

where E_{wp} is the targeted workplace illuminance. The light loss factor (*LLF*) was assumed at 0.8. The coefficient of utilization (*CU*) was 0.8. Table 3 summarizes the energy data of the lighting system. With the lamp efficacy of 100 lumen/W_{elec}, the lighting power density of providing the workplane illuminance at 200 lux, 300 lux, and 500 lux was 4.2, 6.3, and 10.5 W_{elec}/m^2, respectively.

Table 3. Energy data of the LED lamp.

Light output of a lamp (lumen/lamp)	2680		
Power consumption of a lamp (Welec/lamp)	26.8		
Luminous efficacy (lumen/Welec)	100		
Workplane illuminance (lux)	200	300	500
Lighting power density (Welec/m^2)	4.2	6.3	10.5

This study assessed the energy performance of two lighting schemes:

Scheme 1: Only electric lighting with uniform light distribution

Regardless of the interior daylight availability, the LED lamps operated at their rated power to maintain a consistent light flux output throughout office hours. The lighting power density (LPD) was 10.5 Welec/m2 to meet the workplane illuminance at 500 lux.

Scheme 2: Daylighting and task-ambient lighting integration

Dimmable LED lamps were presently uncommon for commercial offices. However, this study hypothesized that the LED lamps could regulate the artificial light flux to supplement the entering daylight. The lighting power density (*LPD*) was proportional to the instant light flux output.

To further reduce lighting energy, the task-ambient lighting concept was applied. The LED lamps and daylight from the windows provided ambient lighting of 300 lux for the entire room (27.0 m^2). An additional light of 200 lux was supplied by table lamps to achieve a total of 500 lux at the workstation. According to Table 3, the lighting power density of the table lamps at the workstation (LPD_{ws}) was 4.2 W_{elec}/m^2. In this analysis, the workstation area (A_{ws}) was 5.4 m^2 and was made based on two assumptions: (i) the occupancy rate of the office space was 0.1 person per square meter, and (ii) the area of each workstation was 2.0 m^2. The average lighting power density for the office room could be calculated from

$$LPD = \frac{\sum_{z=1}^{5} (LPD_z \cdot A_z) + (LPD_{ws} \cdot A_{ws})}{A_f}, \quad (28)$$

where A_f is the total room floor area and A_z is the individual of the five zonal areas as illustrated in Figure 6b.

(b) Cooling load

The cooling load (Q_{ac}) was scoped to the thermal load from the window comprising the transmitted solar radiation and the longwave heat gain via convection and radiation mechanisms. The amount of this loads could be determined by the thermal model in Section 2. For the thermal load from the lighting system, it was assumed equal to the lighting power consumption. Equation (29) expresses the mathematical relationship to calculate the cooling load:

$$Q_{ac} = (q_w \cdot A_w) + (LPD \cdot A_f), \quad (29)$$

where q_w is the total heat gain of the window ($W_{th}/m_w{}^2$), as expressed by Equation (18). A_w is the window area (m^2). The *LPD* value can be obtained from Equation (28).

(c) Electricity use

The energy performance improvement was assessed based on the reduction in electric lighting and cooling energy of the room with the PV slats, compared to the typical room case. The electric lighting and cooling energy (*En*) of the two rooms can be calculated from

$$En = \left(LPD + \frac{Q_{ac}}{COP} \right) \cdot Af \cdot H, \tag{30}$$

where *COP* is the coefficient of performance for the cooling, and *H* is the total office hours in a year. In the calculation, the *COP* value was 2.8, and the *H* value was 2340 h.

(d) Thermal comfort

The radiation asymmetry prescribed in ASHRAE standard 55 was used to assess the thermal comfort from the window with PV slats. The asymmetry was defined as the difference between the plane radiant temperatures (ΔT_{pr}) of the two opposite sides of the person, and it can be calculated by Equation (31):

$$\Delta T_{pr} = T_{pr1} - T_{pr2}. \tag{31}$$

In this study, the formula applied to determine the plane radiant temperature was given in Equation (32) [32]. According to the equation, the mean radiant temperature in the equation accounted for the impact of the transmitted radiation from the window.

$$T_{mrt} = \sqrt[4]{\sum_{i=1}^{n} F_{si} \cdot T_i^4 + \frac{\alpha \cdot f_p \cdot E_{wt}}{\varepsilon_s \cdot \sigma}} \tag{32}$$

where F_{si} represents the form factors between the subject and the opaque walls or transparent windows, T_i is the surface temperature, E_{wt} is the transmitted solar radiation, and f_p is the projected area factor.

In the assessment, the value of the radiant temperature opposite to the window (T_{pr2}) was assumed to be 24 °C. The mean radiant temperature of the plane direct to the window (T_{pr1}) was calculated using Equation (32) and the simulated values of the transmitted solar radiation and the window surface temperature obtained from the proposed thermal model of the PV slat system. According to the widow plane configuration and the vertical plane at the occupant position (0.9 m from the window), the form factor of 0.34 was used in the assessment of the radiant asymmetry.

3.3. Simulation-Based Analysis

An annual simulation was conducted to assess energy performance of the PV slats equipped with a south-facing window. The developed model was used to facilitate the assessment according to the parameters in Section 3.2. In the simulation, the mean radiant temperature and room air temperature were assumed to be constant at 24 °C. The hourly records of the solar radiation, daylight illuminance, and outdoor air temperature at our meteorological station were used in the simulations.

(a) Slat adjustment scheme

A monthly adjustment of the slats to the critical angle was proposed to maximize the daylight use and perfectly intercept the sunlight during the office hours from 8:00 to 17:00. According to the slat geometry and the window orientation relative to the sun path at the study site, the adjustment scheme could be presented in Figure 11. The gentle angle tilting between 0 and 30° indicated that the horizontal slats were very effective for the daylighting and solar control in the tropical region where the sun stays overhead for most of the daytime.

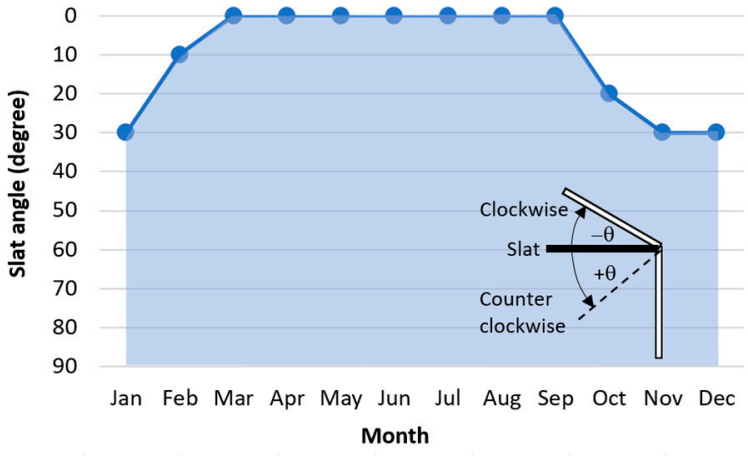
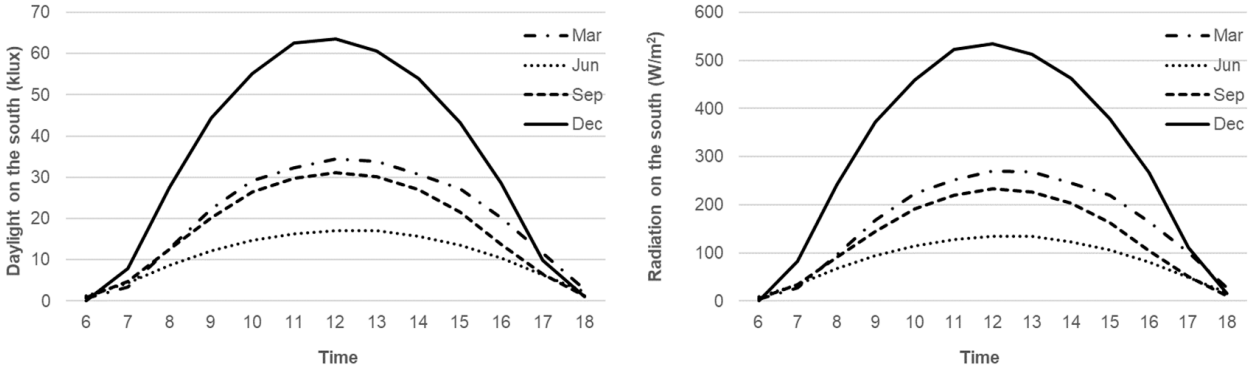


Figure 11. The monthly PV slat adjustment scheme.

(b) Daylight and solar radiation availability

The simulation results were presented for the four selected months: March, June, September, and December. Figure 12a shows the hourly values of the daylight illuminance on the window (south orientation). At the study site location, the sun travels due south from September to April and due north from May to August. The line plots indicated the strong effect of the sun position on the amount of the daylight illuminance.



(**a**) Daylight on the window direction (E_w^v) (**b**) Radiation on the window direction (E_w^s)

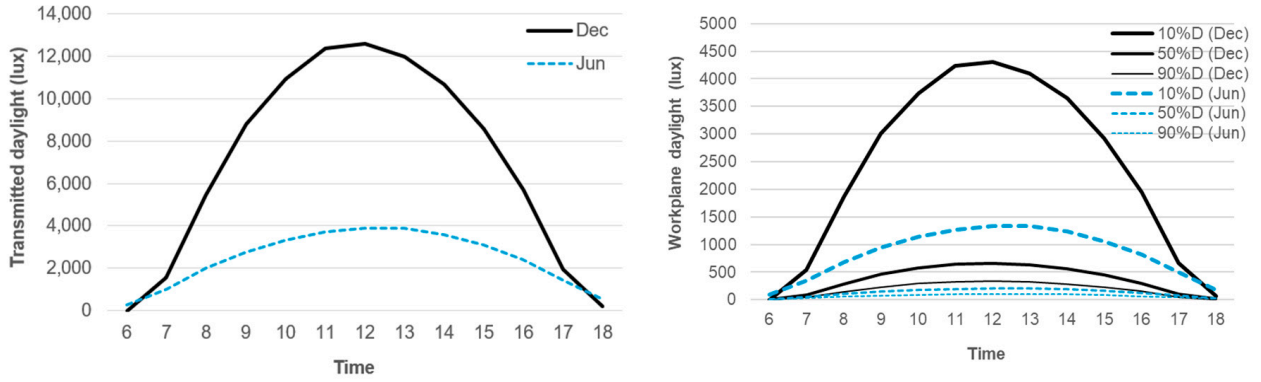
Figure 12. Availability of daylight and solar radiation.

The daylight illuminance was the highest in December when the sun was in front of the window with the lowest elevation. The opposite was true in June when the sun traveled in the back side of the windowed wall and only diffused daylight from the sky presented on the window. In Figure 12b, the corresponding solar radiation was presented a similar variation pattern to the daylight illuminance. From both figures, the daylight illuminance peaked at 60 klux, while the radiation value was about 550 W_{th}/m^2. It is also observed that the daylength was long (12 h a day) and almost equal throughout a year.

(c) Transmitted and workplane daylight

Figure 13a exhibits the amount of daylight that could be transmitted from the double-pane window ($E^v_{t,win}$) with the perfect sun shading. Now, only the results of the two extreme months, i.e., June and December, were picked for presentations. The maximum transmitted daylight increased from 4.0 klux in June to 12.5 klux in December; even in this year-end month, the slats had the steepest shading angle (30°) to shade the sunlight. The transmitted amounts were about 20–23 percent of the available daylight on the window-

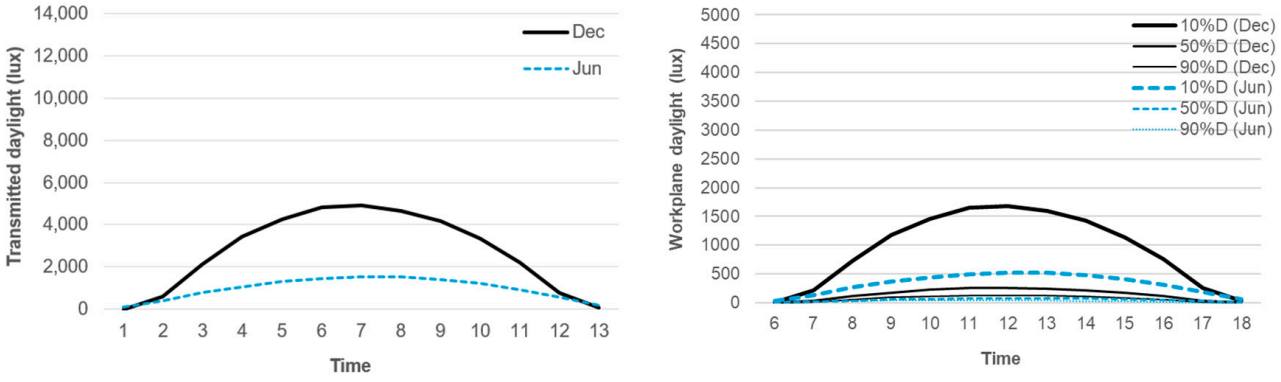
facing façade (south orientation). According to our simulations, the transmitted daylight in December was about triple that in June.



(**a**) Transmitted daylight (**b**) Workplane daylight

Figure 13. Daylight from the window with the PV slats.

Figure 13b exhibits the workplane daylight distribution from the window with the PV slats. The daylight illuminance had an exponentially decreasing trend from the windowed wall to the rear wall. At 10% of the room depth, the workplane daylight varied from about 1000 lux in June to 4000 lux in December throughout the office hours, which was sufficient for task lighting at a workstation. Deepening to 50% of the room depth, the workplane daylight was still sufficient most of the time for general lighting (300 lux); however, the potential would be less at 90% of the room depth. Additional light from table lamps was thus inevitably required to meet the standard lighting requirements of 500 lux at the workstation. For comparison, Figure 14 shows the transmitted daylight from the heat reflective glass window with no sun shading. Due to the very low visible transmittance, the transmitted daylight was quite low. The workplane daylight seemed to have some potential for the area nearby the window.



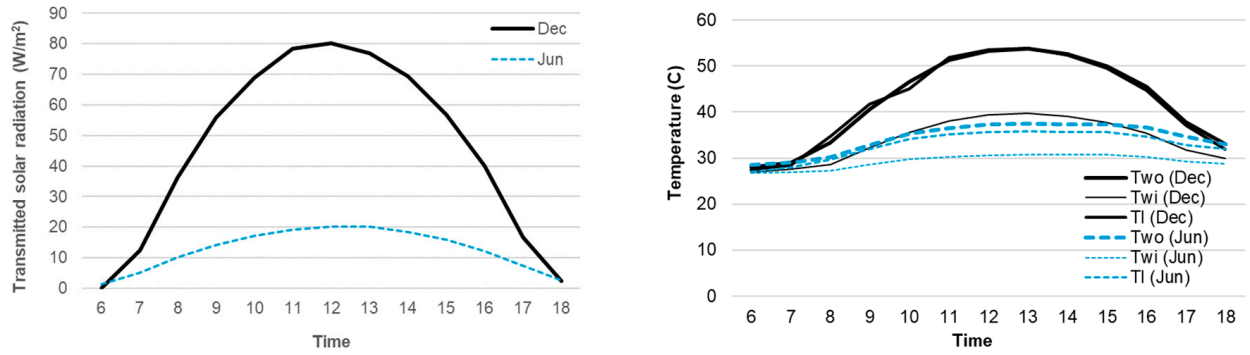
(**a**) Transmitted daylight (**b**) Workplane daylight

Figure 14. Daylight from the heat reflective glass.

(d) Solar and thermal gain

Based on the exterior solar radiation (see Figure 12b), the monthly average values of the transmitted solar radiation from the window with the PV slats is presented in Figure 15a. The transmitted radiation was as high as 80 W_{th}/m^2 in December and was only one-fourth of that in June. The variation pattern was similar to the transmitted daylight. Figure 15b shows the plots of the surface temperature of the windowpanes. During the office hours, the slat and glass temperature values were higher than the ambient temperature, as they absorbed the solar radiation. From the simulation, the inner glass temperature had a peak

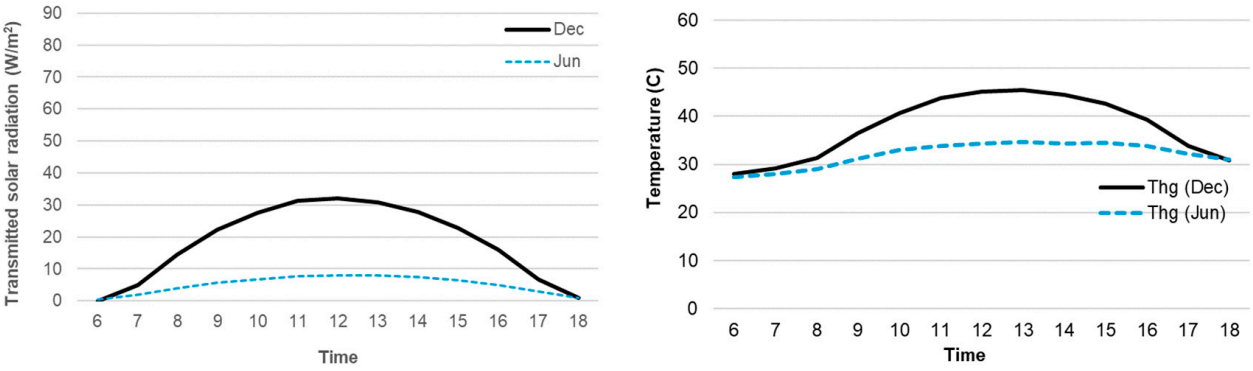
in value in December, reaching 40 °C. However, the peak temperature was only about 30 °C in June.



(**a**) Transmitted solar radiation (**b**) Temperature of the glass window

Figure 15. Thermal gain from the window with slats.

The simulation results of the heat reflective glass were given in Figure 16. Due to the low solar transmittance of the glass, the transmitted radiation was lower compared to that of the double-pane window with the slats. However, it is obvious that the glass would have higher surface temperature than the window glass pane with the PV slats.



(**a**) Transmitted solar radiation (**b**) Temperature of the glass window

Figure 16. Thermal gain from the heat reflective glass.

(e) Energy performance

Table 4 compares the electrical energy for lighting and cooling of the room using the window with the PV slats to the same room using the heat reflective glass window. The first room case also applied the task-ambient lighting concept. As observed, the LED ceiling lamps consumed electricity varying from 3.1 kWh_{elec}/month to 12.6 kWh_{elec}/month for providing ambient light at 300 lux on the workplane with the daylight supplementation. The table lamps constantly consumed 4.1 kWh_{elec}/month to provide additional light for the workstations. The cooling energy to treat the sensible heat from all electric lamps and the shaded window was from 13.8 to 31.1 kWh_{elec}/month. According to the PV slat adjustment, the electricity from the PV slats was around 0.4–3.0 kWh_{elec}/month. Hence, the total energy consumption from lighting and cooling was 360.2 kWh_{elec}/year. For the latter case (the room using the heat reflective glass window), the total energy consumption was 1116.1 kWh_{elec}/year, with 55.7% from the lighting and 44.3% from the cooling. The results demonstrated that the room with the PV slats could gain 67% of energy saving from both lighting and cooling, as compared to the typical room.

Table 4. Comparison of the lighting and cooling energy consumption of the room with the PV system and typical room using heat reflective glass window (kWh_{elec}).

Month	Room Using the PV Slats and Task-Ambient Lighting					Room Using Heat Reflective Glass		
	Ceiling Lamp	Table Lamp	Cooling System	PV	Total	Ceiling Lamp	Cooling System	Total
Jan	4.4	4.1	26.5	2.5	32.5	51.8	47.9	99.7
Feb	4.5	4.1	23.5	1.5	30.6	51.8	44.8	96.6
Mar	5.9	4.1	18.1	0.8	27.4	51.8	40.2	92.1
Apr	9.8	4.1	14.1	0.6	27.4	51.8	38.6	90.5
May	12.6	4.1	13.8	0.4	30.1	51.8	34.1	85.9
Jun	12.3	4.1	14.1	0.4	30.1	51.8	34.7	86.5
Jul	11.9	4.1	14.1	0.5	29.7	51.8	34.8	86.6
Aug	10.3	4.1	14.0	0.5	27.9	51.8	35.5	87.3
Sep	7.6	4.1	16.4	0.7	27.5	51.8	38.0	89.8
Oct	5.7	4.1	20.3	1.4	28.7	51.8	42.6	94.5
Nov	3.6	4.1	28.0	2.7	33.0	51.8	49.8	101.6
Dec	3.1	4.1	31.1	3.0	35.3	51.8	53.0	104.9
Year	91.6	49.8	233.9	15.1	360.2	622.1	494.0	1116.1

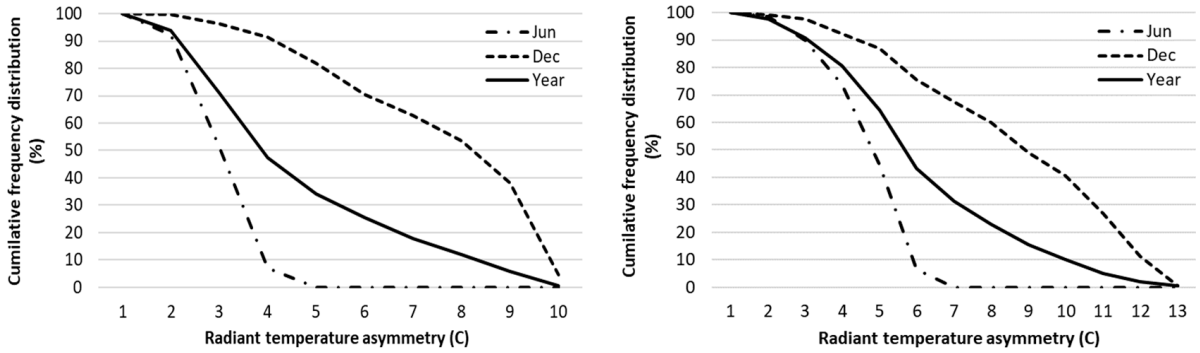
The monthly results in Table 4 show the combined effects of slat angle, solar radiation on the window, and local climate on the energy performance of the PV slat system. As illustrated in Figure 11, the slats were fully open (0 degrees) from March to September to maximize daylight, since the sun is predominantly overhead during these months. However, despite the fully open slats, the ceiling lamps still consumed significant lighting power, implying that less daylight entered the room compared to November through January, when the slats were tilted to 30 degrees for sun shading. It is worth noting that while more daylight entered during November–January; this also brought additional heat gain from solar radiation, potentially offsetting the energy savings from reduced lighting by increasing cooling demands. As a result, the room's monthly energy consumption with the PV slats ranged between 27.4 and 35.3 kWh_{elec}, representing a 65.0–75.2% reduction in energy use compared to the room with heat reflective glass.

(f) Local thermal discomfort

The avoidance of the local thermal discomfort using the window with PV slats was assessed by the lateral radiation asymmetry. Figure 17 exhibits the cumulative distribution plots, indicating the percentage of the frequency at which the plane radiant temperature difference will exceed a given value. In December, when the slats were tilted at 30 degrees to intercept the intense direct solar radiation, the calculated plane radiant temperature difference was at a maximum of 10 °C for the simulated room with the radiant cooling (see Figure 17a). The maximum plane radiant temperature difference did not exceed 5 °C in June, even though the slats were fully open (0-degree tilt). This resulted because the sun stays overhead in this month and only diffuse solar radiation presented on the window plane. In the figure, it was about 35% of the time in a year that the radiant temperature asymmetry would exceed 5 °C.

Considering Figure 17b, the non-shaded heat reflective glass window reached a maximum temperature difference of 13 °C, which was higher than the window with the slats. The occurrence frequency of the temperature difference exceeding 5 °C was as high as 70% over the course of a year. The analysis also exhibited that due to high exterior solar radiation, the occupants next to the window would experience higher local thermal discomfort in December compared to June.

It should be remarked that while this study assessed the energy and comfort performance of the PV slat system, it did not incorporate a cost–benefit analysis, as the initial cost of this system prototype, specifically fabricated for the experiment, could not reflect a realistic commercial price.



(**a**) The window with PV slats (**b**) Heat reflective glass window

Figure 17. Comparison of local discomfort of radiation asymmetry.

4. Conclusions

Both physical experiments and model simulations were carried out to assess the impacts of the adjustable PV slats on the energy use and thermal comfort of an office room equipped with radiant cooling ceiling. The study provided valuable academic insights and deepened the understanding of this technology specifically applied in a tropical environment. The key conclusions are drawn as follows.

A simplified model was introduced for determining the solar transmission and heat transfer of the PV slat system. The model used the incident solar radiation on the windowed wall as the key external variable input, and it could offer the calculation results with acceptable accuracy.

The adjustable horizontal PV slats proved to be a simple and effective solution for enhancing the thermal performance of the south-facing window. Their gentle slope successfully blocked direct sunlight year-round. In our case study, the slats remained at a 0° tilt for seven months (March to September) and were adjusted to 30° for three months (November to January). This adjustment maximized the daylight use while providing large exterior views for the building's occupants.

The application of the PV slats together with the double-pane glazed window and the task-ambient lighting could reduce the office room's annual energy consumption by 67% compared to a typical building design with unshaded heat reflective glass windows. The electricity generated by the PV slats contributed a smaller portion, accounting for approximately 2.0% of the total savings.

The thermal comfort provided by the PV slats was evaluated based on radiation asymmetry in the perimeter zone near the window. By blocking direct sunlight, the slats helped lower the glass surface temperature compared to unshaded heat reflective glass. As a result, the plane radiant temperature difference was minimized, reducing the risk of local discomfort in the radiantly cooled room.

This study introduced a straightforward scheme for monthly slat adjustment. While the mean radiant temperature difference could be aligned with the guidelines of ASHRAE Standard 55, excessive solar and daylight gains were particularly significant during months with lower solar elevation. Optimizing the PV slat angle using Artificial Intelligence (AI) to respond to dynamic outdoor climate conditions could be a crucial next step in advancing this technology, further enhancing window performance and improving overall energy efficiency and thermal comfort in buildings.

Funding: This research project is supported by Thailand Science Research and Innovation (TSRI). Basic Research Fund: Fiscal year 2023 under project number FRB 660073/0164.

Data Availability Statement: The original contributions presented in the study are included in the article, further inquiries can be directed to the author.

Conflicts of Interest: The author declares no conflict of interest.

References

1. United Nations Environment Programme. *2022 Global Status Report for Buildings and Construction: Towards a Zero-Emission, Efficient, and Resilient Buildings and Construction Sector*; United Nations Environment Programme: Nairobi, Kenya, 2022; ISBN 978-92-807-3984-8.
2. Reddy, V.J.; Hariram, N.P.; Ghazali, M.F.; Kumarasamy, S. Pathway to sustainability: An overview of renewable energy integration in building systems. *Sustainability* **2024**, *16*, 638. [CrossRef]
3. Chen, X.; Vand, B.; Baldi, S. Challenges and strategies for achieving high energy efficiency in building districts. *Buildings* **2024**, *14*, 1839. [CrossRef]
4. Raimundo, A.M.; Oliveira, A.V.M. Assessing the impact of climate changes, building characteristics, and HVAC control on energy requirements under a Mediterranean climate. *Energies* **2024**, *17*, 2362. [CrossRef]
5. Freewan, A.A.; Jaradat, N.M.; Amaireh, I.A. Optimizing shading and thermal performances of vertical green wall on buildings in a hot arid region. *Buildings* **2022**, *12*, 216. [CrossRef]
6. Dodoo, A.; Ayarkwa, J. Effects of climate change for thermal comfort and energy performance of residential buildings in a Sub-saharan African climate. *Buildings* **2019**, *9*, 215. [CrossRef]
7. Mohammad, S.T.; Al-Kayiem, H.H.; Aurybi, M.A.; Khlief, A.K. Measurement of global and direct normal solar energy radiation in Seri Iskandar and comparison with other cities of Malaysia. Case Stud. *Therm. Eng.* **2020**, *18*, 100591.
8. Oyewola, O.M.; Patchali, T.E.; Ajide, O.O.; Singh, S.; Matthew, O.J. Global solar radiation predictions in Fiji Islands based on empirical models. *Alex. Eng. J.* **2022**, *61*, 8555–8571. [CrossRef]
9. Chiradeja, P.; Thongsuk, S.; Ananwattanaporn, S.; Ngaopitakkul, A.; Yoomak, S. A study on transparent type envelope material in terms of overall thermal transfer, energy, and economy for an office building based on the Thai Building Energy Code. *Sustainability* **2023**, *15*, 10435. [CrossRef]
10. Sepu'lveda, A.; Salehi, S.S.S.; Luca, F.D.; Thalfeldt, M. Solar radiation-based method for early design stages to balance daylight and thermal comfort in office buildings. *Front. Archit. Res.* **2023**, *12*, 1030–1046. [CrossRef]
11. Hwang, R.L.; Fang, P.L.; Chen, W.A. Impact of solar radiation on indoor thermal comfort near highly glazed façades in a hot-humid subtropical climate: An experimental evaluation. *Build. Environ.* **2023**, *243*, 110725. [CrossRef]
12. Koohsari, A.M.; Heidari, S. Subdivided venetian blind control strategies considering visual satisfaction of occupants, daylight metrics, and energy analyses. *Energy Build.* **2023**, *257*, 111767. [CrossRef]
13. Sherif, A.; Sabry, H.; Wagdy, A.; Mashaly, I.; Arafa, R. Shaping the slats of hospital patient room window blinds for daylighting and external view under desert clear skies. *Sol. Energy* **2016**, *133*, 1–13. [CrossRef]
14. Huo, H.; Xu, W.; Li, A.; Cui, G.; Wu, Y.; Liu, C. Field comparison test study of external shading effect on thermal-optical performance of ultralow-energy buildings in cold regions of China. *Build. Environ.* **2020**, *180*, 106926. [CrossRef]
15. Huo, H.; Xu, W.; Li, A.; Wu, J.; Guo, J. A simple evaluation method of external Venetian blind shading performance for nearly zero energy buildings. *Renew. Energy* **2023**, *218*, 119260. [CrossRef]
16. Ibrahim, A.; Alsukkar, M.; Dong, Y.; Hu, P. Improvements in energy savings and daylighting using trapezoid profile louver shading devices. *Energy Build.* **2024**, *321*, 114649. [CrossRef]
17. Zhang, C.; Gang, W.; Wang, J.; Xu, X.; Du, Q. Experimental investigation and dynamic modeling of a triple-glazed exhaust air window with built-in venetian blinds in the cooling season. *Appl. Therm. Eng.* **2018**, *140*, 73–85. [CrossRef]
18. Lin, Z.; Song, Y.; Chu, Y. Summer performance of a naturally ventilated double-skin facade with adjustable glazed louvers for building energy retrofitting. *Energy Build.* **2022**, *267*, 112163. [CrossRef]
19. Fathoni, A.M.; Chaiwiwatworakul, P.; Mattanant, V. Energy analysis of the daylighting from a double-pane glazed window with enclosed horizontal slats in the tropics. *Energy Build.* **2016**, *128*, 413–430. [CrossRef]
20. Alsukkar, M.; Hu, M.; Alkhater, M.; Su, Y. Daylighting performance assessment of a split louver with parametrically incremental slat angles: Effect of slat shapes and PV glass transmittance. *Sol. Energy* **2024**, *264*, 112069. [CrossRef]
21. Ingabo, S.; Chaiwiwatworakul, P.; Chirarattananon, S. Adjustable external horizontal shading slats for daylighting in office buildings in Thailand. *Asia-Pac. J. Sci. Technol.* **2022**, *27*, 1–10.
22. Ingabo, S.; Chirarattananon, S.; Chaiwiwatworakul, P. Application of external horizontal shading slats for daylighting through slats for daylighting through north-facing windows. *Sci. Eng. Health Stud.* **2021**, *15*, 21040002.
23. Mandalaki, M.; Zervas, K.; Tsoutsos, T.; Vazakas, A. Assessment of fixed shading devices with integrated PV for efficient energy use. *Sol. Energy* **2012**, *86*, 2561–2575. [CrossRef]
24. Oh, S.; Choi, G.-S.; Kim, H. Climate-adaptive building envelope controls: Assessing the impact on building performance. *Sustainability* **2024**, *16*, 288. [CrossRef]
25. Taveres-Cachat, E.; Lobaccaro, G.; Goia, F.; Chaudhary, G. A methodology to improve the performance of PV integrated shading devices using multi-objective optimization. *Appl. Energy* **2019**, *247*, 731–744. [CrossRef]
26. Sanati, L.; Utzinger, M. The effect of window shading design on occupant use of blinds and electric lighting. *Build. Environ.* **2013**, *64*, 67–76. [CrossRef]
27. Gomes, M.G.; Santos, A.J.; Calhau, M. Experimental study on the impact of double tilted Venetian blinds on indoor daylight conditions. *Build. Environ.* **2022**, *225*, 109675. [CrossRef]
28. Togashi, E.; Muramatsu, H.; Nakagawa, J.; Yamada, K. Modeling a solar shading system that controls heat gain by using solar energy to change louver slat angles. *Energy Build.* **2024**, *319*, 114518. [CrossRef]

29. Albuja, R.; Foliaco, B.; Bula, A.; Gonzalez-Quiroga, A. Potential of hybrid radiant cooling with infrared-transparent membranes to improve thermal comfort in hot and humid climate. *Int. J. Thermofluids* **2022**, *16*, 100214. [CrossRef]
30. Aryal, A.; Chaiwiwatworakul, P.; Chirarattananon, S. An experimental study of thermal performance of the radiant ceiling cooling in office building in Thailand. *Energy Build.* **2023**, *283*, 112849. [CrossRef]
31. Lia, J.; Pantelicb, J.; Merchantd, C.B.; Chene, K.W.; Izuharae, I.; Yukif, R.; Meggersd, F.M.; Schiavona, S. Comparison of the environmental, energy, and thermal comfort performance of air and radiant cooling systems in a zero-energy office building in Singapore. *Energy Build.* **2024**, *318*, 114487. [CrossRef]
32. Marino, C.; Nucara, A.; Peri, G.; Rizzo, G.; Scaccianoce, C. The spatial evaluation of the radiative human body heat exchanges: An effective contribution for limiting energy consumption and achieving better indoor conditions in buildings. *J. Build. Eng.* **2023**, *16*, 118–128. [CrossRef]
33. Gao, S.; Yang, L.; Shi, M.; Zhao, S.; Zhou, X.; Zhai, Y. Human thermal comfort under lateral radiant asymmetries. *Energy Built Environ.* **2023**, *4*, 432–444. [CrossRef]
34. Diaconu, B.; Cruceru, M.; Anghelescu, L. A quantitative metric for the indoor environment radiative field asymmetry developed through numerical simulation of the radiative field structure. *J. Build. Eng.* **2021**, *44*, 103345. [CrossRef]
35. *ANSI/ASHRAE Standard 55-2017*; Thermal Environmental Conditions for Human Occupancy. American Society of Heating Refrigerating and Air-Conditioning Engineers Inc.: Atlanta, GA, USA, 2017.

Disclaimer/Publisher's Note: The statements, opinions and data contained in all publications are solely those of the individual author(s) and contributor(s) and not of MDPI and/or the editor(s). MDPI and/or the editor(s) disclaim responsibility for any injury to people or property resulting from any ideas, methods, instructions or products referred to in the content.